Macromolecules

pubs.acs.org/Macromolecules Article

Effect of Synthesis Temperature on Size, Structure, and Volume Phase Transition of Polysaccharide Microgels

Krista G. Freeman, Jacob Adamczyk, and Kiril A. Streletzky*

Cite This: https://dx.doi.org/10.1021/acs.macromol.0c01605 Read Online

ACCESS | Metrics & More | Article Recommendations | Supporting Information

ABSTRACT: High-molecular-weight polysaccharide microgels were synthesized at a range of temperatures above the polymer lower critical solution temperature (LCST) (ΔT = 0.6−18.1 °C), and ΔT was found to strongly influence the structure, dynamics, and volume phase transition temperature of the resulting particles. Static and dynamic light scattering studies and mean field theory analysis of the microgels below and above volume phase transition revealed several distinct regimes. At small ΔT, lower density, larger, and more polydisperse microgels that deswell by a factor 10 in volume were synthesized. At intermediate ΔT = 5−8 °C, the formed microgels were the smallest, densest, and most monodisperse below the transition, but exhibited deswelling only by a factor of 5 above the transition. Synthesis at high ΔT led to the formation of nonuniform microgels with small density, a high degree of polydispersity, and in some cases the apparent presence of the un-cross-linked polymer. Furthermore, the volume phase transition temperature dropped significantly as ΔT increased. This work suggests that synthesis temperature can be used to tune the size, deswelling capacity, and volume phase transition temperature of the polymeric microgels.

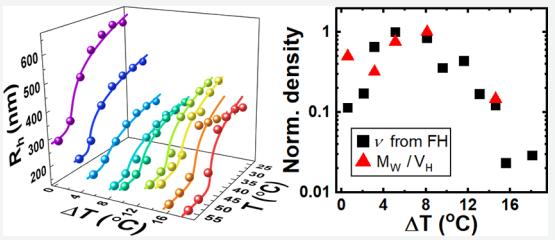

INTRODUCTION

Microgels are environmentally responsive nanoparticles synthesized by cross-linking colloidal aggregates of amphiphilic polymer chains above the lower critical solution temperature (LCST).[1] The cross-linking reaction creates inter- and intrachain chemical bonds, which keep the polymers in close contact, even when the solution temperature drops below the LCST. Unable to dissociate like loose polymer aggregates at low temperatures, synthesized microgels instead swell as they absorb solvent in a volume phase transition below the transition temperature, T_V; above T_V, microgels expel solvent and deswell. This environmentally responsive reversible volume phase transition, which is rapid[2] due to microgels' small size, has been used as a model to study thermodynamic theories of the polymer and gel transitions.[3] It has also been utilized in various applications including biosensing and controlled drug delivery and release.[4] From a drug delivery perspective, microgels' submicron size is well suited for uptake into macrophages via phagocytosis,[5−8] making them a promising candidate for delivery vesicles to these critical drug targets.

The most highly characterized microgel system is synthesized from *N*-isopropylacrylamide (NIPAM) monomers, which are simultaneously polymerized and cross-linked to form poly(*N*-isopropylacrylamide) (PNIPAM) microgels.[1,9] These microgels are typically monodisperse, small, and can deswell to a hundredth of their swollen volume,[1] but their biomedical promise is tempered by the carcinogenic or teratogenic nature of the parent monomers.[10] Another widely studied system of microgels is based on poly(*N*-vinylcaprolactam) (PVCL), a biocompatible synthetic polymer with LCST in the physiological range.[11] As an alternative to synthetic microgels, Lu et al.[12] developed microgels from a natural polysaccharide, hydroxypropyl cellulose (HPC). HPC is an amphiphilic, water-soluble, and neutral polymer with LCST ∼ 41 °C.[13,14] The polymer is already used as an FDA-approved food emulsifier[15,16] and drug encapsulator,[17,18] so it presents an advantage over synthetic polymers for therapeutic use. The HPC microgels themselves were shown to be potentially suitable nanoparticle candidates for tissue augmentation,[19] while providing a good platform for various mechanisms of controlled release of biomolecules.[17]

Knowledge of the internal structure of the microgels is of great importance for understanding and controlling their deswelling behavior. Many studies on PNIPAM and PVCL microgels have highlighted the nonuniform density[20,21] of the microgel particles as probed by SANS,[22] static light scattering (SLS) spectroscopy,[23] and ^{1}H NMR.[11] A widely used model of the nonuniform density microgels is the "fuzzy sphere",[22] a subset of core−corona models in which a constant density core is surrounded by a corona whose density gradually decays to a surface that has dangling chains attached to it. This and similar

Received: July 12, 2020
Revised: October 5, 2020

https://dx.doi.org/10.1021/acs.macromol.0c01605
Macromolecules XXXX, XXX, XXX−XXX

heterogenous microgel structure models successfully describe the behavior not only of many synthesized microgels[11,24] but also of microgels assembled *in silico*.[25−27] In both cases, the density profiles of the microgels with different cross-linking density were studied below and above the volume phase transition. A common finding of these studies is that the density of the corona changes more than the density of the core during the transition.[26]

Compared with PNIPAM and PVCL microgels, however, the literature on HPC microgels is relatively sparse. Lu et al.[12] synthesized HPC microgels with surfactant and probed the dependence of microgel size on the polymer and surfactant concentration, cross-linker density, and synthesis temperature. Ref 12 and similar studies[28] showed that the structure and dynamics of these surfactant-containing microgels are determined by the balance between polymer chain hydrophobic interactions and electrostatic repulsion between surfactant micelles self-assembled on the polymer chains. The balance was found to be somewhat dependent on synthesis temperature, T_{syn}: microgel size distribution widened and slightly grew with an increase of $\Delta T = T_{syn} - \text{LCST}$ as stronger hydrophobic interactions led to larger particles, which in turn led to stronger microgel electrostatic repulsion.

Various studies on surfactant-free HPC microgels[15,29−31] probed the dependence of microgel size on salt and polymer concentrations and, to a limited degree, on synthesis temperature. However, to our knowledge, the effect of ΔT on the surfactant-free HPC microgels has not been systematically studied beyond ref 29, where the role of T_{syn} on microgel size distribution was probed, but was somewhat complicated by the use of NaCl in microgel synthesis. The authors found that the microgel average size increased and its distribution widened with increase of ΔT up to 3 °C for microgels synthesized at a constant salt concentration, indicating faster salt association at higher ΔT that leads to a broader size distribution. However, the authors also found that the microgels synthesized at a fixed temperature but with varying NaCl concentration (an effective change in ΔT, since salt weakens the hydrogen bonding between the polymer and water, lowering LCST) decreased in average size and became more polydisperse with an increase in NaCl. Therefore, the isolated role of T_{syn} on microgel formation is masked in ref 29 by the presence of salt.

On the other hand, the effect of T_{syn} on the microgel structure is expected to be significant. Gao et al.[15] studied the formation of the HPC aggregates at various T and, based on the results, developed a synthesis protocol for the HPC microgels. They found that un-cross-linked HPC chains formed colloidal aggregates above LCST (~41 °C) that were metastable until solution temperature $T > 50$ °C. The structure and dynamics of these HPC aggregates varied significantly with T. As T incrementally increased above LCST, the aggregate size, density, and molecular weight increased, while the width of their size distribution first decreased until about 44 °C and then started to grow significantly. Above 50 °C, the aggregates became kinetically unstable and eventually precipitated. These results are attributed to the interplay, at $T >$ LCST, between polymer phase separation (via intrachain collapse and interchain association) and steric repulsion that keeps polymer aggregates kinetically stable. While their study focused largely on the effect of T on the polymer aggregates, Gao et al.[15] also completed microgel synthesis at one T and found that both size and density increase as the polymer aggregates are subjected to cross-linking to form microgel particles. Given the demonstrated strong effect of T on the un-cross-linked polymer aggregates, it seems important to also have a detailed understanding of its influence on the resulting microgels.

This paper describes the systematic light scattering study of the salt- and surfactant-free HPC microgels synthesized at a large range of temperatures in an attempt to understand the role of T_{syn} on microgel size, structure, and volume phase transition temperature. The next section introduces the experimental methods and data analysis techniques used. The third section presents the experimental results and their discussion. The fourth section brings together the findings of the study in the form of brief conclusions.

EXPERIMENTAL METHODS

Materials. Dry hydroxypropyl cellulose (HPC) powder (nominal M_W values of 100, 300, and 1000 kDa) and divinyl sulfone (DVS) were purchased from Aldrich Chemical Co. Sodium hydroxide (NaOH) pellets were purchased from Fisher Scientific. All materials were used as received. Water for all synthesis purposes and sample preparation was distilled and deionized (resistance of 18MΩ) using a Millipore Milli-Q Academic system.

Spectrophotometry. UV-Vis spectrophotometer (Genesys 10S) was used to measure the absorbance of an HPC solution at each M_W. The experiment utilized a quartz cuvette and a single-cell Peltier (SPG-1A, ThermoFisher) to hold the solution at a particular temperature (within ±0.1 °C). The polymer solutions were studied between 37 °C and 47 °C with step size as small as 0.1 °C near the transition and solutions were given enough time (~10 min) to equilibrate at each T. The steepest part of the increase in absorbance with T for each polymer solution was linearly fit to yield the transition temperature (Figure 1). The intercept of this fit with the level of

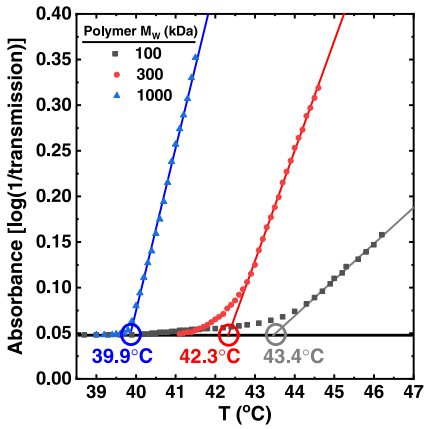

Figure 1. Absorbance as a function of solution temperature (T) for three molecular weights of HPC.

background absorbance was used as the experimental LCST (T_C) for each polymer solution (the values of T_C for each M_W appear in Figure 1 and in Table SI.1). The spectrophotometry results were also checked with dynamic light scattering (DLS) by monitoring the count rate of the scattered light as a function of T.

Microgel Synthesis and Sample Preparation. A 0.05 wt % (0.5 g/L) aqueous HPC solution was prepared and allowed to dissolve by gentle stirring for 1 week. Microgel synthesis began by heating 20 mL of the HPC solution to the synthesis temperature, $T_{syn} > T_C$ (T_C = 39.9 °C for 1000 kDa HPC, Figure 1), in a glass round-bottom flask immersed in a hot water bath and stirred constantly with a magnetic stir bar. After equilibrating at T_{syn}, the flask was removed from the bath (at this point, the solution was cloudy, indicating that the polymer had gone through the dewetting transition) and allowed to cool, then inserted back into the bath, allowed to equilibrate again

https://dx.doi.org/10.1021/acs.macromol.0c01605
Macromolecules XXXX, XXX, XXX−XXX

at T_{syn}, and mixed with 33.3 μL of neat DVS (final DVS concentration ~0.2 wt % or ~16.7 mM). After 2 h, 0.5 mL of 2 M NaOH was added to the solution, raising the pH to ~12 to begin the cross-linking reaction. The solution was incubated at T_{syn} for a further 24 h, then removed from the bath, allowed to cool, and dialyzed against water (using dialysis tubing of MWCO: 6000−8000) to remove NaOH and excess DVS. Dialysis was carried out for at least a week, with at least four water changes, before the synthesized microgel solution was removed from dialysis tubing and, without dilution, filtered through cellulosic filters (pore diameter of 5 μm) into a precleaned and dried borosilicate glass light scattering sample cell. This sample cell was used for both dynamic and static light scattering experiments. Every microgel sample was synthesized in this way, but each with a different $\Delta T = T_{syn} - T_C$. ΔT values ranged from 0.6 to 18.1 °C.

Because the samples were not diluted before analysis, the mass concentration of the microgels is the same as the concentration of the polymer during synthesis (0.05% by weight, or 0.5 g/L). The microgel particle number concentration (particles/L) was estimated as $c_{microgels} = c_{polymer} \times N_A/M_{app}$ and, for the 3 samples subjected to SLS, yielded values from 2×10^{14} to 3×10^{15} particles/L.

Light Scattering Characterization of the Microgels. Dynamic light scattering (DLS) spectroscopy was used to study the structure and dynamics of the HPC microgels below and above volume phase transition. Analysis was based on the measured intensity−intensity autocorrelation function, $g^{(2)}(q,t)$

$$g^{(2)}(q, \tau) = \int_0^T I(q, t')I(q, t' + \tau)\mathrm{d}t' \quad (1)$$

where t is the delay time, T is the experiment duration, and q is the magnitude of the momentum transfer vector, with

$$q = \frac{4\pi n}{\lambda}\sin\left(\frac{\theta}{2}\right) \quad (2)$$

Here, n is the index of refraction of the solvent, λ is the wavelength of light in vacuum, and θ is the scattering angle.

A field correlation function, $g^{(1)}(q,t)$ was obtained from $g^{(2)}(q,t)$ using the Siegert relation and then analyzed by fitting the function to a sum of stretched exponentials:

$$g^{(1)}(q, t) = \sum_{i=1}^{N} A_i \mathrm{e}^{(-t/\tau_i)^{\beta_i}} \quad (3)$$

here A_i, τ_i, and β_i are the amplitude, decay pseudo-time, and stretching parameter of the ith mode, with N being the number of modes. All of the microgel correlation functions were found to be represented accurately by one or, in the case of the two highest ΔT samples, two stretched exponential modes. While this representation of $g^{(1)}(q,t)$ is not necessarily unique, it produces small root mean square (RMS) errors and reproducible results. Spectral time moment analysis[14,32] then allowed to directly deduce the zeroth spectral time moment M_0 from $g^{(1)}(q,t)$. In fact, due to the functional form of $g^{(1)}(q,t)$, M_{0i} can be calculated analytically for each mode

$$M_{0i} = \int_0^\infty \mathrm{e}^{(-t/\tau_i)^{\beta_i}}\mathrm{d}t = \gamma(1 + 1/\beta_i)\tau_i \quad (4)$$

where $\gamma(1+n) = n!$ is the γ function, which should be distinguished from a spectral decay rate Γ. Each zeroth time moment yields mean relaxation time of an exponential decay; therefore, a mean decay rate $\langle\Gamma_i\rangle$ of a relaxation can be found as $\langle\Gamma_i^{-1}\rangle \equiv M_{0i}/0!$. A corresponding mean diffusion coefficient D_i for a given relaxational mode can be found from $D_i = \langle\Gamma_i\rangle/q^2$.

For dilute spherical particles in a small-molecule, low-viscosity solvent, the measured mean diffusion coefficient, D, can be directly related to the hydrodynamic radius, R_H, of the particle via the Stokes−Einstein equation

$$D = \frac{k_B T}{6\pi\eta R_H} \quad (5)$$

Here, k_B is Boltzmann's constant, T is the absolute temperature of the solvent, and η is the solvent viscosity. Equation 5 is not valid for nonspherical particles, highly polydisperse solutions, and in concentrated solutions.

Static light scattering (SLS) spectroscopy was employed to measure weight-average molecular weight, M_W, and radius of gyration, R_g, of the microgel samples. The SLS experiment is based on the angular (θ) dependence of the average intensity of scattered light $I(\theta)$ with analysis following the Rayleigh−Gans−Debye approximation. Since measured SLS spectra showed significant nonlinearity, the data was analyzed with the Berry plot (instead of Zimm)

$$\left(\frac{Kc}{R}\right)^{1/2} = \left(\frac{1}{M_W}\right)^{1/2}\left(\left(1 + \frac{q^2R_g^2}{6}\right) + 2A_2cM_W \ldots\right)^{1/2} \quad (6)$$

Here, c is the concentration of the particles in the solution, A_2 is the second virial coefficient, and $K = \frac{4\pi^2 n^2\left(\frac{dn}{dc}\right)^2}{N_A\lambda^4}$ is the optical constant related to the solvent's index of refraction n (water, 1.33), the solutions' specific refractive increment dn/dc (0.164 cm^3/g for HPC water solution at 30 °C, from Hormnirun et al.[33]), the wavelength of the scattered light in vacuum, λ (514.5 nm), and Avogadro's number N_A. R in eq 6 is the excess Rayleigh ratio given by $R_{std}\frac{(I(\theta) - I_s(\theta))\sin\theta}{I(90)_{std}}\left(\frac{n}{n_{std}}\right)^2$ where R_{std} is the Rayleigh ratio of the standard, n_{std} is the index of refraction of the standard, $I(90)_{std}$ is the 90-degree scattered intensity of the standard, and $I_s(\theta)$ is the scattered intensity by the solvent. For these SLS experiments, carbon disulfide was used as a standard. Its index of refraction and Rayleigh ratio were extrapolated from the literature[34−38] to be n_{std} =1.64 and $R_{std}(90) = 1.1793 \times 10^{-4}$ cm^{-1} at λ = 514.5 nm.

All of the light scattering experiments employed an Ar$^+$ laser (Stabilite 2017, Spectra Physics) at a wavelength of 514.5 nm with an output power of up to 2 W. Optics, consisting of neutral density attenuator (Model 925B Newport), irises, and lenses, were carefully aligned together with photometer-goniometer (BI-200SM, Brookhaven Instruments) to assure that the incoming light went through the center of the cylindrical sample cell placed into a decalin-filled index matching vat. A 200 μm pinhole was used in front of the detector for DLS and 1 mm pinhole for SLS measurements. The DLS spectra were analyzed by an ALV-5000 correlator, while the goniometer arm was controlled by a BI-9000 correlator. The SLS photon count rate was collected using a BI-9000 correlator as well. The cell holder was maintained within 0.1 °C of the desired temperature by a refrigerated circulating bath (Neslab, RTE-111). The transition temperature experiments were performed at 90°. The angular dependence of $g^{(2)}(q,t)$ was mostly studied between 30 and 105°, with a step of 5°. For several samples, the angular range of DLS was extended to 130°. SLS measurements were performed using the same optical setup in the range of angles 30 and 120° with an angular step of 2°.

RESULTS AND DISCUSSION

Figure 2 shows typical normalized intensity−intensity correlation functions for a 1000 kDa HPC-based microgel sample synthesized at ΔT = 2.1 °C at a range of solution temperatures, T, above and below the volume phase transition. These correlation functions are unimodal and cover almost three decades of a decay—the quality of these curves is representative of all samples in this study, with the exception of two samples (discussed later). Figure 2 reveals a consistent increase in the decay rate of correlation functions Γ with an increase in T from 25 to 55 °C. Fitting these correlation functions according to eq 3 and using spectral time moment analysis[14,32] yields the diffusion coefficient and corresponding hydrodynamic radius, R_H, as a function of T, as shown in the inset to Figure 2. The inset highlights the process of microgel

https://dx.doi.org/10.1021/acs.macromol.0c01605
Macromolecules XXXX, XXX, XXX−XXX

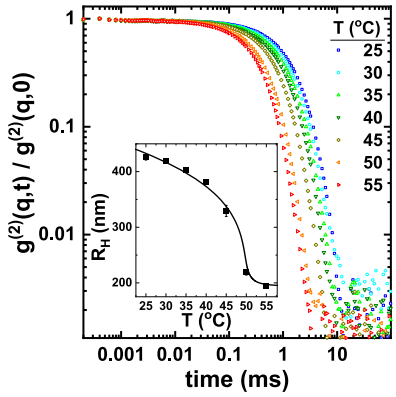

Figure 2. Normalized correlation functions for a typical microgel (ΔT = 2.1 °C) at a range of solution temperatures, T, from 25 to 55 °C. The inset shows corresponding R_H as a function of T and fit with the Flory-Rehner model.

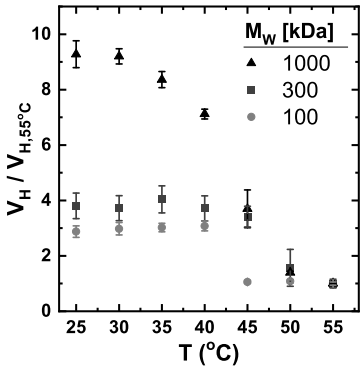

Figure 3. Hydrodynamic volume of microgels at a given temperature normalized by microgel hydrodynamic volume at 55 °C as a function of solution temperature, T, for three microgels synthesized with HPC of different M_W.

volume phase transition with an increase of solution temperature.

The primary objective of this project was to explore the effect of synthesis temperature on microgel particles by characterizing their size, deswelling ability, and structure. To assess subtle changes in synthesized microgel structure and dynamics, preliminary studies were performed to identify a system with a large dynamic range of sizes. To this end, the effect of the polymer molecular weight (M_W, ranging from 100 to 1000 kDa) on microgel size above and below the volume phase transition was assessed. Absorbance experiments shown in Figure 1 reveal that the polymer's dewetting transition temperature, T_C, decreases with increasing molecular weight. Using this data, the microgels were synthesized at $\Delta T \sim 1.5-2.1$ °C (namely, 1.5 °C for 100 kDa; 1.7 °C for 300 kDa; and 2.1 °C for 1000 kDa). The synthesized microgels were then studied by single-angle (90°) DLS experiments at a range of temperatures.

DLS experiments showed that, in the swollen state (at 25 °C), microgel size (Figure SI.1, Supporting Information) increases with an increase in M_W. This is logical, as the longer chains of high M_W should have a greater ability to expand and contract than the shorter chains of low M_W. Conversely, for the deswollen microgels (at 55 °C), an increase in M_W yields a decrease in microgel size. These trends suggest that the largest volume swelling ratio, and thus the largest (and most useful for this study) range of particle sizes, could be obtained with the microgels synthesized at the highest M_W. Indeed, Figure 3 plots the solution temperature dependence of the normalized hydrodynamic volume, $V_H/V_{H,55\,°C}$, which shows that the swelling ratio increases with M_W increase. Figure 3 also indicates that the sharpness of the volume phase transition depends on the polymer M_W. The microgels from M_W = 100 kDa HPC show a sharp transition, while higher M_W microgels have a broader transition. This effect may be caused by a broader distribution of polymer chain lengths at larger M_W. Since chain length influences the T_C[39] (see Figure 1), this greater polymer polydispersity could lead to more heterogeneity of the chains comprising microgel particles and, thus, to a broader volume phase transition in the microgels synthesized from the higher M_W polymer.

Based on the results shown in Figure 3, the parent polymer with M_W = 1000 kDa was chosen for the synthesis temperature study because these microgels exhibited the largest dynamic range of sizes, allowing subtle changes across samples to be quantified with light scattering. A series of microgels were synthesized from the 1000 kDa HPC with T_{syn} varied from 40.5 to 58 °C, corresponding to $\Delta T = T_{syn} - T_C$ of 0.6−18.1 °C. In Figure 4A, the hydrodynamic radius obtained from 90° scattering, R_H, is plotted against T for the range of ΔT, illustrating the volume phase transition for each synthesized microgel. The results show that the microgels deswell from 300 to 625 nm at 25 °C down to 140−300 nm at 55 °C, with both swollen and collapsed sizes strongly depending on ΔT. Indeed, the largest microgels both below and above T_V were produced at the smallest ΔT of 0.6 °C. The swollen microgel size decreases as ΔT increases until ΔT = 5.1−8.1 °C, where the R_H hits a minimum of 300−350 nm in the swollen state and 170−190 nm in the deswollen state. As ΔT increases above 8.1−14.6 °C, the R_H of the synthesized microgels grows below the transition to ∼450 nm while remaining ∼200 nm in the deswollen state. This dependence of R_H on ΔT can also be seen on the inset of Figure 4A and in the three-dimensional (3D) representation of R_H vs ΔT and T (Figure SI.2).

As was noted earlier, the measured correlation functions at all but two highest ΔT were unimodal up to 2.5−3 orders of decay both below and above the transition temperature (as seen in Figures 2 and 4B). At the two highest ΔT, on the other hand, the correlation functions were strongly bimodal (Figure 4C-top) below the transition, with the second mode contributing as much as 20% to the decay (for 90° scattering). The bimodal fits yielded somewhat noisy R_H for the main (faster mode) shown in Figures 4A and SI.2. In contrast, the unimodal fits of these highly bimodal correlation functions produced poor fits (as seen from the residuals on Figure 4C-top) and, therefore, were not used. On the other hand, above the volume phase transition, the correlation functions (CF) even at the highest ΔT were unimodal (Figure 4C-bottom, with the second mode appearing only after 2.5 orders of CF decay). This suggests that the slow mode seen below the transition could be attributed to un-cross-linked polymer chains in the solution, which join the formed microgels above T_V.

In addition to the overall particle size, synthesis temperature also affects microgels' degree of deswelling, as shown in Figure 5. For microgels synthesized at small ΔT, the hydrodynamic volume changes by a factor of 8−10 between the swollen (25 °C) and collapsed (55 °C) states. In comparison, the intermediate ΔT samples (5.1 and 8.1 °C) deswell more

https://dx.doi.org/10.1021/acs.macromol.0c01605
Macromolecules XXXX, XXX, XXX−XXX

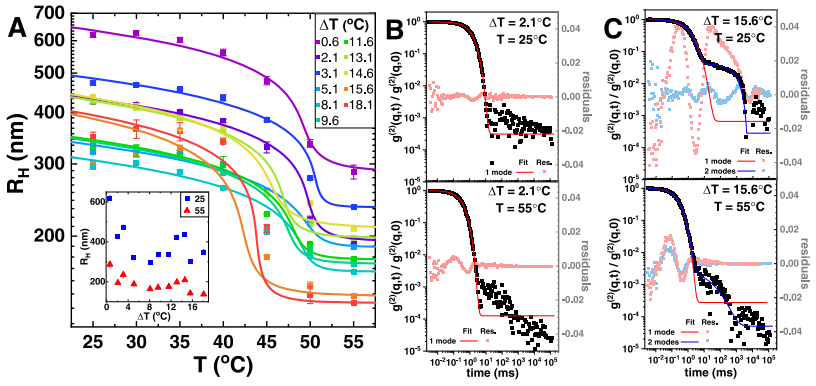

Figure 4. (A) R_H as a function of solution temperature T for all synthesis temperatures ΔT. The solid lines are fits to eq 7, which are discussed later. The inset plots $R_H(\Delta T)$ at 25 and 55 °C. Normalized correlation functions below and above the transition temperature for: (B) ΔT = 2.1 °C with unimodal fits and residuals and (C) ΔT =15.6 °C with unimodal and bimodal fits and corresponding residuals.

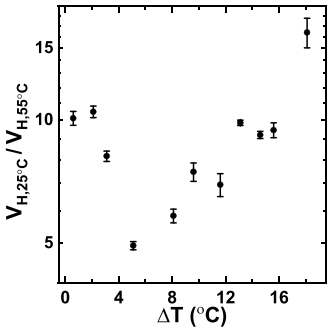

Figure 5. Hydrodynamic volume, V_H, of the swollen microgels at 25 °C normalized by the hydrodynamic volume of the deswollen microgels at 55 °C as a function of ΔT.

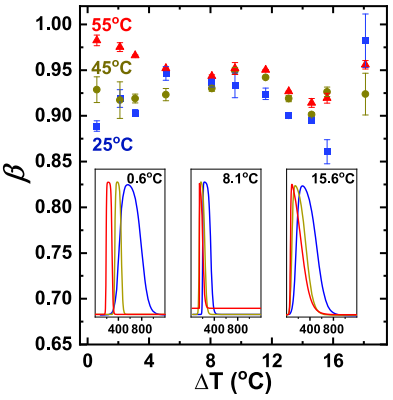

Figure 6. Stretching parameter of the fits, β, at 90° as a function of ΔT for the microgels at T = 25, 45, and 55 °C. The inset: CONTIN size distribution at T = 25, 45, and 55 °C for three representative microgels (low ΔT = 0.6 °C, intermediate ΔT = 8.1 °C, and high ΔT = 15.6 °C).

modestly, by a factor of 5−6. As ΔT increases above 8.1 °C, microgel's degree of deswelling increases, with a volume ratio of up to 16 (the $V_{H,25\,°C}$ estimate for the two samples at the highest ΔT came from the first mode of strongly bimodal correlation functions). This effect of synthesis temperature on the degree of deswelling of the HPC microgels can be compared to the behavior of the micron-sized PNIPAM microgels[40] where an increase of T_{syn} led to microgels with a larger degree of swelling.

The effect of synthesis temperature on the stretching parameter, β, obtained from the 90° correlation function fits to eq 3 is shown in Figure 6. All values of β came from the unimodal fits, except for the 25 °C data at two highest ΔT where β came from the dominant faster mode of the bimodal fit. β values of 1 are representative of monodisperse spherical particles, while lower values of β indicate polydispersity in the sample. At low ΔT, the swollen particles (at 25 °C) are relatively polydisperse ($\beta \sim 0.9$), while the collapsed particles (at 55 °C) are essentially monodisperse ($\beta > 0.96$). At intermediate ΔT, β is somewhat lower than at low ΔT in the collapsed state and stays roughly unchanged at 0.92−0.95 below and above the transition. At high ΔT, both swollen and collapsed particles are relatively more polydisperse, with single-mode β falling below 0.92 with an increase of ΔT until it behaves unpredictably at the two highest ΔT values (where the spectra were bimodal). The size distributions (inset of Figure 6) obtained from CONTIN analysis of the correlation functions reveal similar polydispersity trends. Indeed, the size distributions of the microgels synthesized at intermediate ΔT (8.1 °C) are consistently narrower than the size distributions of the microgels synthesized at low and high ΔT both below and above the transition. These trends hold at all solution temperatures.

Multiangle DLS experiments on the microgels synthesized at $0.6 \le \Delta T \le 14.6$ °C yielded more detailed information about the particles' structure and dynamics. Figure 7 plots the correlation function decay rate Γ (defined after eq 4) as a function of q^2 for the microgels of various ΔT both below and

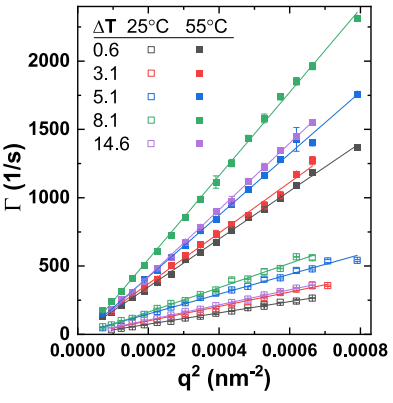

Figure 7. Γ vs q^2 for the microgels synthesized at various ΔT below (25 °C) and above (55 °C) the volume phase transition.

https://dx.doi.org/10.1021/acs.macromol.0c01605
Macromolecules XXXX, XXX, XXX−XXX

above the volume phase transition. All studied microgels show linear $\Gamma(q^2)$ dependence with negligible intercepts (see Table SI.2 for the linear fit parameters and derived R_H values) for all T up to $q^2 = 6.5-8 \times 10^{-4}$ nm^{-2}, indicating that all prepared microgels behave as diffusive particles as a whole. The high ΔT microgels shown in Figure 7 have slight deviations from $\Gamma/q^2 =$ const (Figure SI.3, Supporting Information), which are consistent with a soft sphere model[41] or core−corona models with a soft exterior.[22] Again, none of the correlation functions used in Figures 7 and SI.3 were bimodal.

To further explore microgel structure and dynamics, the SLS experiments were performed for the representative microgel samples (with ΔT = 0.6, 5.1, and 14.6 °C) over a range of solution temperatures. The optical settings were kept the same during these experiments to eliminate the changes in scattering intensity caused by sources other than the sample, allowing for direct qualitative and quantitative comparisons of each curve. Figure 8A shows the Berry plots for a subset of experimental

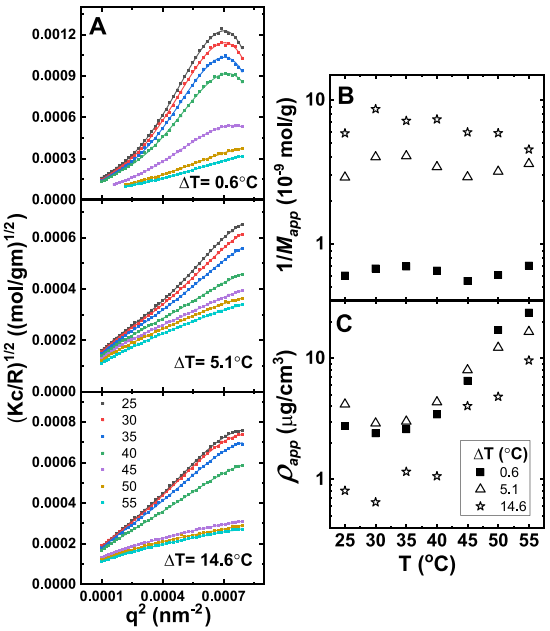

Figure 8. SLS results for three microgels with different ΔT: (A) Berry plots with corresponding fits at a range of T from 25 to 55 °C for the microgels synthesized at ΔT of 0.6, 5.1, and 14.6 °C. The results for the samples ΔT of 0.6 °C (■), 5.1 °C (△), and 14.6 °C (☆): (B) T-dependence of inverse apparent molecular weight, $1/M_{app}$, and (C) T-dependence of apparent microgel density ρ_{app}.

data with corresponding fits. At ΔT = 0.6 °C, there is a significant curvature of the $(Kc/R)^{1/2}(q^2)$ dependence at $T < T_V$, a consequence of the large swollen particle size. The curvature decreases as the particles deswell with an increase of solution temperature, with a large jump as T exceeds T_V. The curvature essentially disappears at 55 °C, when the particles are fully collapsed. Similar trends are evident at other ΔT. The degree of curvature also strongly depends on ΔT: at $T<T_V$, the microgels synthesized at ΔT of 0.6 °C have the most significant $(Kc/R)^{1/2}(q^2)$ curvature, the ΔT = 5.1 °C sample has the least $(Kc/R)^{1/2}(q^2)$ curvature, and the ΔT = 14.6 °C sample is somewhere in between (these trends may be easier to appreciate in Figure SI.4, where the curves are plotted on a 3D graph). This suggests that ΔT has a strong effect on swollen microgel size and structure. In particular, the smallest change in the curvature of $(Kc/R)^{1/2}(q^2)$ with T for ΔT = 5.1 °C indicates that this sample undergoes a relatively minor change in size and structure upon deswelling. Thus, this figure qualitatively illustrates the structural landscape of the microgels, with the large, lower density, highly dynamic particles at extreme values of ΔT contrasted by the small, dense, and relatively unchanging particles at the intermediate ΔT plateau.

The curves also yield quantitative structural information through fits. As shown in eq 6, the squared intercept of the Berry plot is $1/M_W + 2A_2c = 1/M_{app}$, where M_{app} is the apparent molecular weight at a finite concentration. Analysis of the fits shows (Figure 8B) that $1/M_{app}$ increases with increasing ΔT, but is largely independent of T (at least at low and intermediate ΔT). This indicates that the microgels at lower ΔT have the higher M_{app}, which stays roughly constant (or decreases slightly) with an increase of solution temperature. At the highest ΔT (14.6 °C), the microgels have a lower M_{app}, which increases by more than 30% with increasing T. It is possible that M_{app} for this sample is somewhat underestimated at low T due to a large contribution from interparticle interactions (large A_2). Alternatively, it is possible that M_{app} does actually increase due to un-cross-linked or long dangling chains that get incorporated into the microgels above the volume phase transition. Figure 8C shows the apparent average density ($\rho_{app} = M_{app}/V_H$) as a function of T for the microgels shown in Figure 8A. For each microgel, the apparent average density increases several folds during the deswelling transition. The increase in average density with a change in T from 25 to 55 °C is the smallest at intermediate ΔT = 5.1 °C (a factor of ∼4) and the largest at high ΔT = 14.6 °C (a factor of ∼12.5), reflecting the significant changes in V_H and small changes in M_{app}. Figure 8C also shows that the microgels synthesized at ΔT = 14.6 °C are the least dense at all T, while the microgels made at ΔT = 5.1 °C are the densest particles, at least below the volume phase transition. Again, these apparent densities depend on M_{app}, which may be underestimated due to interparticle interactions. Therefore, the trends in Figure 8C may also reflect the degree of interparticle interaction between the microgels as a function of synthesis temperature (i.e., microgels with very high ΔT would appear to have stronger interparticle interactions). The estimates of the average ρ_{app} do not consider possible core−corona architecture of the microgels, in which the core and corona may have very different densities. Such an architecture may explain the finding that ρ_{app} for ΔT = 14.6 °C is ∼5 times smaller than that of the other ΔT at 25 °C but only ∼2 times smaller at 55 °C. Such a result is consistent with literature[26] findings that the corona size changes more than the core size during volume phase transition. It may be that this sample (ΔT = 14.6 °C) has a larger and less dense corona than the other samples.

As a second measure of the relative particle density, the DLS data was analyzed with the Flory-Rehner (FR) mean field theory to obtain an estimate of the particle density for each ΔT. The Flory-Rehner equation (eq 7), derived from mixing entropy and elastic free energy,[42−44] was used to relate solution temperature, T, and the fractional size of the microgel particles, φ:

$$T = \frac{\Delta H}{k_B\left(\frac{v_1\nu}{N_A\varphi^2}\left[\left(\frac{\varphi}{\varphi_0}\right) - 2\left(\frac{\varphi}{\varphi_0}\right)^{1/3}\right] - \frac{2}{\varphi} - \frac{2\ln(1-\varphi)}{\varphi^2}\right) + \Delta S} \quad (7)$$

https://dx.doi.org/10.1021/acs.macromol.0c01605
Macromolecules XXXX, XXX, XXX−XXX

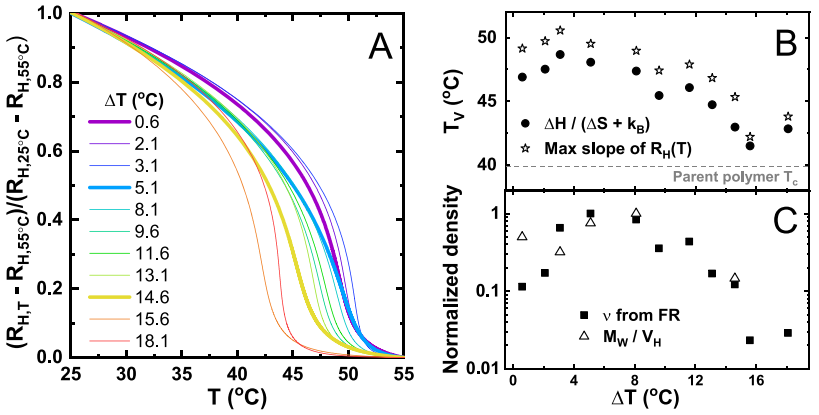

Figure 9. (A) FR fits for normalized $R_H(T)$ dependences for all ΔT. (B) Temperature dependence of T_V from $\frac{\Delta H}{\Delta S + k_B}$ (●) and from the maximum slope of FR fits (☆). (C) Two normalized measures of relative microgel density as a function of ΔT: number of chains per microgel volume from FR fits (■), ν, and the apparent average microgel mass density from combined SLS (M_W) and DLS (R_H) (△) at 25 °C.

In this equation, k_B is Boltzmann's constant, N_A is Avogadro's number, ν_1 is the molar volume of solvent (0.018L/mol for water), and φ_0 is the volume fraction in the reference state, which we estimate (following refs[29,45]) by $V_{H,55\,°C}/V_{H,25\,°C}$ (see Table SI.3 for a list of φ_0 values). The fitting parameters in eq 7 (assuming no draining conditions with $R \approx R_H$) are the enthalpy of mixing, ΔH, entropy of mixing, ΔS, and the density as the number of polymer chains per particle volume, ν. Equation 7 is written for the case of no ionic contribution to free energy (since HPC is neutral, and there is no salt in our system) and for Flory polymer−solvent interaction parameter, χ, being approximated by $\frac{\Delta H - T\,\Delta S}{2k_B T}$ (see a graph of $\chi(\Delta T)$ at several T in Figure SI.5). The fits were performed, unconstrained, using a user-defined fitting function in Origin Graphing and Analysis software, which was iterated until the fit converged. These fits are shown as the solid lines to the R_H vs T data in Figure 4A.

Xia et al.[29] has considered a similar free-energy thermodynamics approach for the HPC microgels synthesized in the presence of NaCl. There, the authors fixed the value of ν (4×10^{24} L^{-1}, an estimate based on the HPC:DVS molar ratio) and fit $R_H(T)$ curves to obtain ΔS (-1.76×10^{-20} J/K) and ΔH (-5.56×10^{-18}J). In the present work, the polymer chain density ν was considered to be a variable, resulting in values (5.7×10^{23} to 2.5×10^{25} L^{-1}, depending on T_{syn}), which generally agree with Xia et al. Additionally, the values of $-\Delta H$ obtained here range from 0.5−2.1 $\times 10^{-18}$ J, and the values of $-\Delta S$ range from 1.7 to 6.5 $\times 10^{-21}$ J/K (see Table SI.3 for all fit parameters). It should be noted that these values of $-\Delta S$ (and to a lesser extent, $-\Delta H$) are smaller than those in Xia et al.[29] for the HPC microgels with salt and also smaller than the established value of -1.8×10^{-20} J/K for PNIPAM-type gels.[45] The discrepancy in the HPC microgels can be partially attributed to additional microstates available in the case of Xia et al.[29] due to the presence of salt in their microgel solutions and hence larger expected entropy of mixing. It should also be noted that while FR formalism is generally considered to describe well the swelling of the highly cross-linked microgels,[44] the accuracy of the fitting parameters is harder to assess[46] due to model limitations and differing definitions of the reference state in the presence of solvent.[44] That said, even if the absolute values of these fit parameters are not accurate, the trends as a function of ΔT are still meaningful and can provide insight into the effect of ΔT on microgel structure.

As seen from Figure 4A, the Flory-Rehner model describes well the experimentally observed microgel volume phase transitions and yields two important results. First, the FR fits provide a measure of the volume phase transition temperature, T_V. Indeed, Figure 9A shows normalized FR fits of $R_H(T)$ at various ΔT, revealing a shift of the steepest part of the FR fitting lines toward lower temperature with an increase in ΔT. It is also evident that the shape of these curves varies with ΔT. In other words, both positioning (along T) and the sharpness of the swelling−deswelling curves depend on synthesis temperature (contrary to some findings on the PNIPAM microgels[40]). T_V can be estimated by finding the maximum slope of the FR fitting lines. Alternatively, T_V of each sample can be calculated through the ratio of $\frac{\Delta H}{\Delta S + k_B} = T_V$.[44] These two measures are shown in Figure 9B and differ somewhat, with $\frac{\Delta H}{\Delta S + k_B}$ consistently 0.7−2.4 °C lower than the maximum slope estimate. This is expected, as $\frac{\Delta H}{\Delta S + k_B}$ is an estimate of the θ temperature and thus marks the beginning of the volume phase transition. The maximum slope estimate, on the other hand, indicates the temperature at which the particle undergoes the most dramatic deswelling due to increased hydrophobic interactions.

Figure 9B also shows that both estimates of T_V decrease by ∼5 °C, nearly monotonically, as ΔT increases, starting at ∼47 and 49 °C ($\frac{\Delta H}{\Delta S + k_B}$ and maximum slope measures, respectively) for low ΔT and falling to ∼43 and 44 °C for high ΔT. This result suggests that microgel synthesis at higher ΔT results in particles with volume phase transition temperature T_V closer to parent polymer's T_C. In other words, similar to ionic strength,[12,45,47] synthesis temperature can seemingly be used to tune the trigger point of the microgel volume phase transition.

The second important result of the FR fits is that it provides an estimate of the number of chains per particle volume, ν, for the microgels at various ΔT. Figure 9C plots the normalized values of ν as a function of ΔT and compares it to the normalized apparent mass density ($\rho_{app} = M_{app}/V_H$, as in Figure 8C) obtained from the combination of SLS and DLS in the swollen state at 25 °C. Both independent estimates of

https://dx.doi.org/10.1021/acs.macromol.0c01605
Macromolecules XXXX, XXX, XXX−XXX

relative microgel particle density agree in revealing a strong dependence on synthesis temperature. Both show a well-pronounced maximum at the intermediate ΔT = 5.1−8.1 °C. Below and above the intermediate ΔT, microgel particle density is relatively small. This is especially true for the microgels synthesized at large ΔT. These particles are more than an order of magnitude less dense than those synthesized at the intermediate ΔT, according to both Flory-Rehner model and DLS/SLS experiments, which seems to suggest that more inhomogeneous microgels have lower ν, consistent with the literature.[40]

The results presented here suggest that microgel synthesis temperature strongly impacts the size, density, and structure of the formed microgels. This is likely due to the effect of temperature on the degree of HPC dewetting: higher T_{syn} correlates with more thermal kinetic energy in the system and results in more hydrogen bonds being broken, leading to larger hydrophobic forces, which drive the polymer into, on average, denser aggregates. The density of the polymer aggregates during synthesis determines the extent of cross-linking within the formed microgels, and the cross-linking density determines the extent to which the particles can deswell at low temperatures.

As a result, at very low ΔT (just above T_C), the polymer aggregates during synthesis should still be somewhat hydrophilic and thus very loosely condensed, with a small hydrophobic core and long hydrophilic arms. This loose packing would result in a less dense cross-linking network and, at the conclusion of synthesis, a softer, less dense, and more polydisperse population of the swollen microgel particles. This scenario would be consistent with core−corona or fuzzy sphere models with a smaller core. At intermediate ΔT, however, hydrophobic forces dominate and the polymer aggregates during synthesis are denser and more compact. Such aggregates, with many close contacts between the chains, would be subject to a large degree of cross-linking. This dense cross-linking network would, in turn, limit the capacity of the particle to swell when temperature drops below T_V. This is supported by the observations here that the swollen microgels of intermediate ΔT are smaller, more monodisperse, and have higher apparent average density and smaller density change upon deswelling than their counterparts with low ΔT. These findings would be consistent with the microgels whose dense core is bigger, while corona is smaller. At high ΔT, the polymer clusters are subjected to even stronger hydrophobic forces, but may be unable (due to volume exclusion) to further condense. It is possible that these very strong hydrophobic forces drive uncontrolled and nonuniform polymer aggregation. One potential result is the assembly of the compact, well-ordered aggregates formed at intermediate ΔT into bulky and irregular clusters of the aggregates. There may also be instances of single-polymer chains collapsing onto themselves and their immediate neighbors, but not being incorporated into the larger polymer aggregates. Alternatively, the corona of the microgels at these ΔT may significantly grow in size with more dangling chains attached on the periphery. These scenarios could explain the observations that the swollen microgels of high ΔT are quite polydisperse, larger on average, and have a smaller apparent density than other microgels. These particles would exhibit apparent signs of internal microgel dynamics due to nonuniform distribution of the polymer chains in the microgels. Finally, for the two samples synthesized with the highest ΔT (15.6 and 18.1 °C), the bimodal correlation functions below (but not above) the volume transition indicate a significant presence of the un-cross-linked polymer chains. Perhaps the cross-linker does not have enough time to diffuse uniformly through the volume during synthesis, leading to large and highly polydisperse polymer clusters and a significant amount of un-cross-linked polymer chains. It is also possible that the change of T_{syn} alters the relative HPC collapse and DVS cross-linking kinetics[48] during the synthesis, resulting in particles that are formed when chains are cross-linked in varying degrees of collapse and/or aggregation.

CONCLUSIONS

The effect of synthesis temperature on the structure, dynamics, and volume phase transition temperature of surfactant- and salt-free high-molecular-weight HPC microgels has been studied with light scattering spectroscopy. It was found that by varying $\Delta T = T_{syn} - T_C$ by up to 18.1 °C the microgel size, structure, and density can be tuned. At low ΔT, large, low density, and relatively polydisperse particles are formed below T_V. These particles deswell by a factor of 10 in volume to become monodisperse, ∼10 times denser sphere-like particles above the T_V. At intermediate ΔT, the formed microgels are smaller, but have high density and are relatively monodisperse above and below T_V; they deswell only by a factor of 5 in volume and become denser by a similar amount. At high ΔT, the microgels have properties of lower density, lower mass, and polydisperse swollen particles that remain relatively polydisperse after 10-fold collapse in volume (and ∼12.5-fold increase in density) above T_V. Solutions of these microgels display some properties of internal modes, long dangling chains, and signs of loose polymer chains that did not undergo cross-linking, especially at the highest ΔT. In addition, Flory−Rehner mean field theory analysis of the DLS data supported SLS/DLS findings on the density of the microgels at different ΔT and yielded the dependence of microgel's volume phase transition temperature on ΔT that can be used in designing the microgels with specific T_V.

ASSOCIATED CONTENT

Supporting Information

The Supporting Information is available free of charge at https://pubs.acs.org/doi/10.1021/acs.macromol.0c01605.

Spectrophotometry results for determination of T_C, DLS results for different M_W, 3D representation of R_H vs ΔT and vs T, DLS q-dependence results, 3D representation of the SLS curves as a function of ΔT and T, Flory−Rehner fitting parameters, and dependence of χ on ΔT at several T (PDF).

AUTHOR INFORMATION

Corresponding Author

Kiril A. Streletzky − *Department of Physics, Cleveland State University, Cleveland, Ohio 44115-2214, United States;* orcid.org/0000-0002-0894-5178; Email: k.streletzky@csuohio.edu

Authors

Krista G. Freeman − *Department of Physics, Cleveland State University, Cleveland, Ohio 44115-2214, United States;* orcid.org/0000-0002-2944-5076

Jacob Adamczyk − *Department of Physics, Cleveland State University, Cleveland, Ohio 44115-2214, United States*

https://dx.doi.org/10.1021/acs.macromol.0c01605
Macromolecules XXXX, XXX, XXX−XXX

Complete contact information is available at:
https://pubs.acs.org/10.1021/acs.macromol.0c01605

Author Contributions

The manuscript was written through the contributions of all authors. All authors have given approval to the final version of the manuscript.

Funding

The authors acknowledge CSU's Undergraduate Summer Research Award for support of K.G.F, 2020 CSU's Faculty Research Development award for support of K.A.S., and National Science Foundation grant (REU Award no. 1659541) for support of J.A.

Notes

The authors declare no competing financial interest.

■ ACKNOWLEDGMENTS

The authors would like to acknowledge Andrew Scherer for control sample preparations and assistance with fitting DLS correlation functions.

■ REFERENCES

(1) Pelton, R. Temperature-Sensitive Aqueous Microgels. *Adv. Colloid Interface Sci.* **2000**, *85*, 1−33.
(2) Li, Y.; Tanaka, T. Kinetics of Swelling and Shrinking of Gels. *J. Chem. Phys.* **1990**, *92*, 1365−1371.
(3) Wu, C. A Comparison between the ćoil-to-Globule' Transition of Linear Chains and the "Volume Phase Transition" of Spherical Microgels. *Polymer* **1998**, *39*, 4609−4619.
(4) Rapoport, N. Physical Stimuli-Responsive Polymeric Micelles for Anti-Cancer Drug Delivery. *Prog. Polym. Sci.* **2007**, *32*, 962−990.
(5) Pei, Y.; Yeo, Y. Drug Delivery to Macrophages: Challenges and Opportunities. *J. Controlled Release* **2016**, *240*, 202−211.
(6) Tae, H.; Lee, S.; Ki, C. S. *β*-Glucan Hybridized Poly(Ethylene Glycol) Microgels for Macrophage-Targeted Protein Delivery. *J. Ind. Eng. Chem.* **2019**, *75*, 69−76.
(7) Hopkins, S.; Carter, S.; Swanson, L.; MacNeil, S.; Rimmer, S. Temperature-Dependent Phagocytosis of Highly Branched Poly(N-Isopropyl Acrylamide-Co-1,2 Propandiol-3-Methacrylate)s Prepared by RAFT Polymerization. *J. Mater. Chem.* **2007**, *17*, 4022−4027.
(8) Zhou, X.; Su, F.; Tian, Y.; Meldrum, D. R. Dually Fluorescent Core-Shell Microgels for Ratiometric Imaging in Live Antigen-Presenting Cells. *PLoS One* **2014**, *9*, No. e88185.
(9) Wu, C.; Zhou, S. Internal Motions of Both Poly(N-Isopropylacrylamide) Linear Chains and Spherical Microgel Particles in Water. *Macromolecules* **1996**, *29*, 1574−1578.
(10) Harsh, D. C.; Gehrke, S. H. Controlling the Swelling Characteristics of Temperature-Sensitive Cellulose Ether Hydrogels. *J. Controlled Release* **1991**, *17*, 175−185.
(11) Balaceanu, A.; Demco, D. E.; Möller, M.; Pich, A. Microgel Heterogeneous Morphology Reflected in Temperature-Induced Volume Transition and 1H High-Resolution Transverse Relaxation NMR. The Case of Poly(N-Vinylcaprolactam) Microgel. *Macromolecules* **2011**, *44*, 2161−2169.
(12) Lu, X.; Hu, Z.; Gao, J. Synthesis and Light Scattering Study of Hydroxypropyl Cellulose Microgels. *Macromolecules* **2000**, *33*, 8698−8702.
(13) Bu, Z.; Russo, P. S. Diffusion of Dextran in Aqueous (Hydroxypropyl)Cellulose. *Macromolecules* **1994**, *27*, 1187−1194.
(14) Phillies, G. D. J.; Streletzky, K. A. Dynamics of Semirigid Rod Polymers from Experimental Studies, In *Soft Condensed Matter: New Research*; Nova Science: New York, 2007; pp 219−263.
(15) Gao, J.; Haidar, G.; Lu, X.; Hu, Z. Self-Association of Hydroxypropylcellulose in Water. *Macromolecules* **2001**, *34*, 2242−2247.
(16) McDonough, R.; Cueto, R.; Phillies, G. D. J.; Russo, P. S.; Dorman, D.; Streletzky, K. A. Fluorescent Labeling Can Alter Polymer Solution Dynamics. *Macromolecules* **2015**, *48*, 7245−7255.
(17) Cai, T.; Hu, Z.; Ponder, B.; John, J., St.; Moro, D. Synthesis and Study of and Controlled Release from Nanoparticles and Their Networks Based on Functionalized Hydroxypropylcellulose. *Macromolecules* **2003**, *36*, 6559−6564.
(18) Francis, M. F.; Piredda, M.; Winnik, F. M. Solubilization of Poorly Water Soluble Drugs in Micelles of Hydrophobically Modified Hydroxypropylcellulose Copolymers. *J. Controlled Release* **2003**, *93*, 59−68.
(19) Weng, H.; Zhou, J.; Tang, L.; Hu, Z. Tissue Responses to Thermally-Responsive Hydrogel Nanoparticles. *J. Biomater. Sci. Polym. Ed.* **2004**, *15*, 1167−1180.
(20) Saunders, B. R.; Vincent, B. Microgel Particles as Model Colloids: Theory, Properties and Applications. *Adv. Colloid Interface Sci.* **1999**, *80*, 1−25.
(21) Gilányi, T.; Varga, I.; Meszaros, R.; Filipcsei, G.; Zrinyi, M. Characterisation of Monodisperse Poly(N-Isopropylacrylamide) Microgel Particles. *Phys Chem Chem Phys* **2000**, 1973−1977.
(22) Stieger, M.; Richtering, W.; Pedersen, J. S.; Lindner, P. Small-Angle Neutron Scattering Study of Structural Changes in Temperature Sensitive Microgel Colloids. *J. Chem. Phys.* **2004**, *120*, 6197−6206.
(23) Varga, I.; Gilányi, T.; Mészáros, R.; Filipcsei, G.; Zrínyi, M. Effect of Cross-Link Density on the Internal Structure of Poly(N-Isopropylacrylamide) Microgels. *J. Phys. Chem. B* **2001**, *105*, 9071−9076.
(24) Richtering, W.; Berndt, I.; Pedersen, J. S. Determination of Microgel Structure by Small-Angle Neutron Scattering, In *Microgel Suspensions*; John Wiley & Sons, Ltd: 2011; pp 117−132.
(25) Gnan, N.; Rovigatti, L.; Bergman, M.; Zaccarelli, E. In Silico Synthesis of Microgel Particles. *Macromolecules* **2017**, *50*, 8777−8786.
(26) Rovigatti, L.; Gnan, N.; Zaccarelli, E. Internal Structure and Swelling Behaviour Of in Silico microgel Particles. *J. Phys. Condens. Matter* **2017**, *30*, No. 044001.
(27) Rudyak, V. Y.; Kozhunova, E. Y.; Chertovich, A. V. Towards the Realistic Computer Model of Precipitation Polymerization Microgels. *Sci. Rep.* **2019**, *9*, No. 13052.
(28) Cai, T.; Hu, Z.; Marquez, M. Synthesis and Self-Assembly of Nearly Monodisperse Nanoparticles of a Naturally Occurring Polymer. *Langmuir* **2004**, *20*, 7355−7359.
(29) Xia, X.; Tang, S.; Lu, X.; Hu, Z. Formation and Volume Phase Transition of Hydroxypropyl Cellulose Microgels in Salt Solution. *Macromolecules* **2003**, *36*, 3695−3698.
(30) Streletzky, K. A.; McKenna, J. T.; Mohieddine, R. Spectral Time Moment Analysis of Microgel Structure and Dynamics. *J. Polym. Sci. Part B: Polym. Phys.* **2008**, *46*, 771−781.
(31) Streletzky, K. A.; McKenna, J. T. Spectral Time Moment Analysis of Microgel Deswelling. Effect of the Heating Rate. *J. Polym. Sci. Part B: Polym. Phys.* **2008**, *46*, 2792−2802.
(32) Phillies, G. D. J.; O'Connell, R.; Whitford, P.; Streletzky, K. A. Mode Structure of Diffusive Transport in Hydroxypropylcellulose:-Water. *J. Chem. Phys.* **2003**, *119*, 9903−9913.
(33) Hormnirun, P.; Sirivat, A.; Jamieson, A. M. Complex Formation between Hydroxypropylcellulose and Hexadecyltrimethylamonium Bromide as Studied by Light Scattering and Viscometry. *Polymer* **2000**, *41*, 2127−2132.
(34) Pike, E. R.; Pomeroy, W. R. M.; Vaughan, J. M. Measurement of Rayleigh Ratio for Several Pure Liquids Using a Laser and Monitored Photon Counting. *J. Chem. Phys.* **1975**, *62*, 3188−3192.
(35) Samoc, A. Dispersion of Refractive Properties of Solvents: Chloroform, Toluene, Benzene, and Carbon Disulfide in Ultraviolet, Visible, and near-Infrared. *J. Appl. Phys.* **2003**, *94*, 6167−6174.
(36) Bello, A.; Guzman, G. M. Light Scattering by Pure Solvents. *Eur. Polym. J.* **1966**, *2*, 79−83.
(37) Deželić, G. Evaluation of Light-Scattering Data of Liquids from Physical Constants. *J. Chem. Phys.* **1966**, *45*, 185−191.

(38) Finnigan, J. A.; Jacobs, D. J. Light Scattering from Benzene, Toluene, Carbon Disulphide and Carbon Tetrachloride. *Chem. Phys. Lett.* **1970**, *6*, 141−143.
(39) Koningsveld, R.; Staverman, A. J. Liquid−Liquid Phase Separation in Multicomponent Polymer Solutions. II. The Critical State. *J. Polym. Sci. Part 2: Polym. Phys.* **1968**, *6*, 325−347.
(40) Habicht, A.; Schmolke, W.; Lange, F.; Saalwächter, K.; Seiffert, S. The Non-Effect of Polymer-Network Inhomogeneities in Microgel Volume Phase Transitions: Support for the Mean-Field Perspective. *Macromol. Chem. Phys.* **2014**, *215*, 1116−1133.
(41) Burchard, W. Static and Dynamic Light Scattering from Branched Polymers and Biopolymers, In *Light Scattering from Polymers*; Advances in Polymer Science; Springer: Berlin, Heidelberg, 1983; pp 1−124.
(42) Flory, P. J. *Principles of Polymer Chemistry*; Cornell University Press: Ithaca, 1953.
(43) Flory, P. J.; Rehner, J. Statistical Mechanics of Cross-Linked Polymer Networks II. Swelling. *J. Chem. Phys.* **1943**, *11*, 521−526.
(44) Quesada-Pérez, M.; Maroto-Centeno, J. A.; Forcada, J.; Hidalgo-Alvarez, R. Gel Swelling Theories: The Classical Formalism and Recent Approaches. *Soft Matter* **2011**, *7*, 10536−10547.
(45) Hirotsu, S.; Hirokawa, Y.; Tanaka, T. Volume-phase Transitions of Ionized N-isopropylacrylamide Gels. *J. Chem. Phys.* **1987**, *87*, 1392−1395.
(46) Lopez, C. G.; Richtering, W. Does Flory-Rehner Theory Quantitatively Describe the Swelling of Thermoresponsive Microgels? *Soft Matter* **2017**, *13*, 8271−8280.
(47) Del Monte, G.; Ninarello, A.; Camerin, F.; Rovigatti, L.; Gnan, N.; Zaccarelli, E. Numerical Insights on Ionic Microgels: Structure and Swelling Behaviour. *Soft Matter* **2019**, *15*, 8113−8128.
(48) Elaissari, A.; Mahdavian, A. R. Polymerization Kinetics of Microgel Particles, In *Microgel Suspensions*; John Wiley & Sons, Ltd: 2011; pp 33−51.

https://dx.doi.org/10.1021/acs.macromol.0c01605
Macromolecules XXXX, XXX, XXX−XXX